Available online at www.sciencedirect.com
SCIENCE DIRECT®
Comput. Methods Appl. Mech. Engrg. 193 (2004) 4223–4245
Computer methods in applied mechanics and engineering
www.elsevier.com/locate/cma

An ALE formulation based on spatial and material settings of continuum mechanics. Part 2: Classification and applications

Harm Askes [a], Ellen Kuhl [b], Paul Steinmann [b,*]

[a] Faculty of Civil Engineering and Geosciences, Delft University of Technology, P.O. Box 5048, NL-2600 GA, Delft, The Netherlands
[b] Faculty of Mechanical Engineering, University of Kaiserslautern, P.O. Box 3049, D-67653 Kaiserslautern, Germany

Received 16 May 2003; received in revised form 29 August 2003; accepted 4 September 2003

Abstract

In the second paper of this two-part contribution, a specialisation towards Neo–Hookean material will be made of the generic hyperelastic arbitrary Lagrangian–Eulerian (ALE) formulation derived in Part 1. First, for the sake of comparison and classification, several existing ALE solution schemes are discussed, including total and updated approaches, as well as monolithic and staggered algorithms. Then, implementational details are provided for the newly proposed ALE strategy. The versality and the limitations of the present formulation are shown by means of a set of one-dimensional and multi-dimensional numerical examples. In particular, it is shown that with the proposed ALE formulation, potential energies can be obtained that are minimum for the considered topology.

Keywords: Arbitrary Lagrangian–Eulerian formulation; Spatial and material settings; Variational principle; Spatial and material forces; Finite element method

1. Introduction

In the first part of this contribution [1], an arbitrary Lagrangian–Eulerian (ALE) formulation was derived which is based on the simultaneous solution of the spatial motion problem and the material motion problem. Whereas the notion of the spatial motion problem is well-established (normally known simply as the standard equilibrium equation or the standard equations of motion), the notion of the material motion problem is less obvious. The material motion problem is concerned with the equilibrium of material forces, whereby material forces arise as a result of *material inhomogeneity*, such as defects, voids, (micro-)cracks [2–7]. However, material forces also arise as a consequence of discretisation, as has been exemplified in [8–12]. In fact, on a discretised level there is no difference whether a material force results from a material

* Corresponding author.
E-mail addresses: h.askes@citg.tudelft.nl (H. Askes), ekuhl@rhrk.uni-kl.de (E. Kuhl), ps@rhrk.uni-kl.de (P. Steinmann).

0045-7825/$ - see front matter © 2004 Elsevier B.V. All rights reserved.
doi:10.1016/j.cma.2003.09.031

inhomogeneity or from discretisation. Solving the discretised material motion problem is thus equivalent to minimising spurious material forces stemming from inappropriate discretisations, i.e. to optimise the mesh.

As such, the dual equilibrium problem (solving the spatial motion problem together with the material motion problem) is a mesh optimisation strategy. Both the spatial motion problem and the material motion problem aim at minimising the potential energy. In the spatial motion problem, energy minimisation is performed by finding the optimal *spatial* positions of the nodes, i.e. the positions of the nodes in the spatial configuration. Equivalently, in the material motion problem, energy minimisation is performed by finding the optimal *material* positions of the nodes, i.e. the positions of the nodes in the material configuration. Indeed, the fundamental unknowns of the spatial motion problem and the material motion problem are the spatial and material coordinates of the nodes, respectively.

In the remeshing/adaptivity community, solving for spatial and material coordinates simultaneously is known as the arbitrary Lagrangian–Eulerian approach [13–15]. ALE approaches are not Lagrangian since nodes can move with respect to the material (cf. the material motion problem), neither are they Eulerian since nodes can move in space (cf. the spatial motion problem). Thus, the dual equilibrium problem of spatial motion and material motion is by its very nature an ALE formulation. The dual equilibrium can even be considered as the *ultimate* ALE formulation, since it aims at an absolute minimisation of potential energy, with respect to both the spatial and the material coordinates of the nodes.

In Part 1 of this contribution, the dual equilibrium problem has been derived for the general hyperelastic continuous and discretised case, whereby it has been assumed that an energy potential exists from which the spatial motion problem as well as the material motion problem derive. In the present paper (Part 2), the framework of the dual equilibrium problem will be further elaborated for the hyperelastic case by means of a Neo–Hookean strain energy density. To this end, some basic notions on existing alternative ALE formulations will be revisited in Section 2, including ALE kinematics and various algorithms. In Section 3 the dual equilibrium problem, taken from the first paper [1], is elaborated for the Neo–Hookean case. Section 4 deals with various implementational aspects, paying special attention to simplifications for the one-dimensional case and the incremental-iterative analysis of the dual equilibrium problem. In Section 5, one and two-dimensional examples are treated, showing the advantages and limitations of the proposed ALE formulation.

2. Classification of ALE formulations

This section serves to relate the currently proposed ALE framework to existing and by the meantime classical ALE formulations. ALE methods have originally been devised for application in fluid mechanics, see for instance [13,14] and references cited therein. Later, the extension towards solid mechanics has been made, whereby especially the history-dependence of the material has been paid special attention to [15–17]. Applications with hyperelastic or hyperelastoplastic material have received relatively little attention, notable exceptions being [18–20]. However, it is especially hyperelastic material and its balance laws in spatial and material settings that bear close resemblance to the classical ALE approaches [1,2,12].

2.1. ALE kinematics

For the subsequent discussion of different ALE algorithms, it is necessary to review some of the ALE kinematics (for a complete overview of ALE kinematics, see [13–15]; for a an overview of ALE kinematics in relation to the dual equilibrium problem, see Part 1 of this contribution [1]).

Motion of matter in a Lagrangian formulation is described by mapping a material domain $\mathscr{B}_0$ onto a spatial domain $\mathscr{B}_t$. In an ALE formulation, the nodes of the discretisation can move in space independently of the material, hence a third computational domain is needed. This domain is commonly known as the

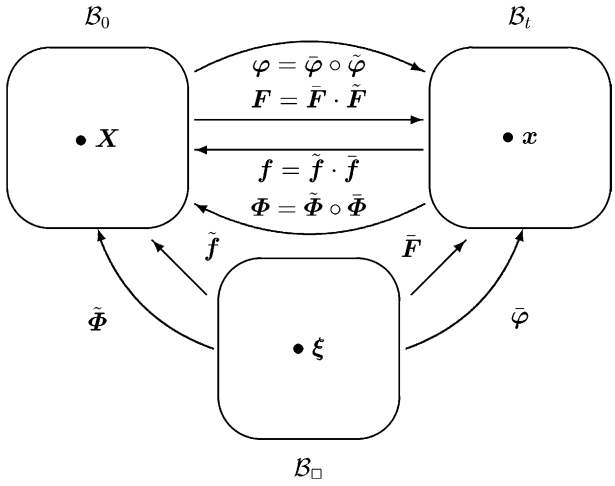

Fig. 1. Reference domain $\mathscr{B}_\square$, material domain $\mathscr{B}_0$ and spatial domain $\mathscr{B}_t$.

reference domain, denoted here as $\mathscr{B}_\square$. The three computational domains are depicted in Fig. 1, together with their respective mappings and deformation gradients. In particular, $\tilde{\boldsymbol{\Phi}}$ maps a node $\boldsymbol{\xi}$ onto a material position $\boldsymbol{X}$ and $\bar{\varphi}$ maps a node $\boldsymbol{\xi}$ onto a spatial position $\boldsymbol{x}$. The usual map between $\boldsymbol{X}$ and $\boldsymbol{x}$ is given by $\varphi = \bar{\varphi} \circ \tilde{\varphi}$, whereas the inverse map between $\boldsymbol{x}$ and $\boldsymbol{X}$ is denoted as $\boldsymbol{\Phi} = \tilde{\boldsymbol{\Phi}} \circ \bar{\boldsymbol{\Phi}}$. The relevant deformation gradients are written as $\boldsymbol{F}$, $\boldsymbol{f}$, $\overline{\boldsymbol{F}}$ and $\tilde{\boldsymbol{f}}$, respectively.

The introduction of a third domain has two important implications. Firstly, the nodal positions are introduced as unknowns and they must be solved for (see Section 2.4). Secondly, time updates, if present, change when a Lagrangian description is rewritten into an ALE description. This last issue is treated in detail in classical references on ALE techniques [13–15]; the resulting equation is listed here simply as

$$\left.\frac{\partial \mathscr{F}(\boldsymbol{X},t)}{\partial t}\right|_{\boldsymbol{X}} = \left.\frac{\partial \mathscr{F}(\boldsymbol{\xi},t)}{\partial t}\right|_{\boldsymbol{\xi}} + \left.\nabla_{\boldsymbol{x}} \mathscr{F}(\boldsymbol{x},t)\right|_{t} \cdot \boldsymbol{c} \tag{1}$$

in which $\mathscr{F}$ is an any physical property and $\boldsymbol{c}$ is the so-called convective velocity, i.e. the velocity with which the nodes of the mesh and the material particles diverge. The notation $|_a$ means 'keeping a fixed'. Thus, Eq. (1) should be understood as follows: the time derivative of $\mathscr{F}$ in a Lagrangian context (i.e. keeping $\boldsymbol{X}$ fixed) equals the time derivative of $\mathscr{F}$ in an ALE context (i.e. keeping $\boldsymbol{\xi}$ fixed) *plus* the contribution of the convection—this convective contribution is proportional to the convective velocity $\boldsymbol{c}$ and to the spatial gradient of $\mathscr{F}$.

Notice that convective terms only appear when time updates are involved and are thus no issue in this contribution. Convective terms require special care in a numerical context. In the assessment of different ALE algorithms, the presence or absence of convective terms is an important issue.

2.2. Total ALE versus updated ALE

In the previous section, a reference domain has been introduced that is related to the mesh. A crucial aspect of this reference domain is that it should be independent of the material domain, but otherwise the user is free to select it. Typically, in a numerical context, two options would appear as particularly convenient, namely (i) to take the initial configuration as the reference configuration, or (ii) to take the configuration of the previous step as the reference configuration. Analogous to classical large strain

formulations of solid mechanics, these two options are referred to as Total ALE (or T-ALE) and Updated ALE (or U-ALE), respectively.

Remark 1 (*Terminology*). The acronym U-ALE has been used in the literature as well to denote iterative schemes in which the material coordinates of the nodes are determined once per time step [21]. This issue will be treated in more detail in Section 2.3.

The choice between T-ALE and U-ALE carries important implications, as has been emphasised recently [19]. In particular, when a T-ALE approach is chosen, the nodal coordinates of the initial configuration must be stored, which is not necessary in case a U-ALE approach is taken. On the other hand, in a U-ALE approach the relation between the position of an integration point in the current configuration and its position in the initial configuration is lost, therefore every time the mesh is moved, the state variables have to be transported [19].

Now, two issues should be taken into consideration: the format of the constitutive update (total versus incremental) and the mappings between the three computational domains (spatial, material and referential). If the constitutive update is written in its total form like in the present hyperelastic case, no time derivatives appear, hence no convection needs to be accounted for in the constitutive equation, cf. Eq. (1). On the other hand, if the constitutive update is written in an incremental (or rate) format, the time derivatives would have to be rewritten by means of Eq. (1), leading to convective terms. In short, T-ALE schemes are compatible with total constitutive updates in the sense that neither of them results in the appearance of convective terms [18,19]. In contrast, both U-ALE schemes and incremental formats of the constitutive relations necessarily lead to convective terms and require a transport algorithm for the state variables [15,19,22,23].

Another issue concerns the quality of the mappings between the spatial, material and reference domain. Indeed, this has been one of the original motivations of using ALE approaches, namely to avoid excessive distortion of the mesh, i.e. to improve the mapping between reference domain and spatial domain. In general, it can be said that large differences between the various domains may lead to singularities in the corresponding mappings, and this must be avoided by a proper adaptive strategy. In a classical T-ALE approach, the three domains are entirely independent of each other. This implies that upon excessive deformations, large differences may arise between the three domains, and the quality of *two* mappings must be controlled by the user: the mapping between material domain and reference domain, and the mapping between spatial domain and reference domain. On the other hand, in a U-ALE approach, the difference between the material domain and the reference domain will be relatively small, since the reference domain coincides with the material domain of the previous load step. Thus, only the quality of the mapping between reference domain and spatial domain needs special care. In summary, the requirements put on the remeshing by a T-ALE approach are much more strict and less likely to be fulfilled than those put by a U-ALE approach.

The choice between T-ALE or U-ALE is elaborated for three different cases:

(1) In ALE applications with infinitesimal strains, the mapping between material domain and spatial domain remains of the initial quality. In other words, the mappings between material domain and reference domain on the one hand and between spatial domain and reference domain on the other hand are virtually identical. Thus, as far as maintaining the quality of mappings is concerned, the difference between T-ALE and U-ALE becomes irrelevant. Since the mapping between material domain and spatial domain poses no problems, the remeshing strategy can be entirely devoted to mesh refinement in zones of interest [23–28].
(2) In ALE applications with large strains *but with elastic material behaviour*, T-ALE approaches have the advantage that no convective terms appear, but the quality of two mappings must be controlled [18,19].

In contrast, U-ALE schemes lead to convective terms, but only one mapping needs to be controlled. Thus, the selection of either a T-ALE scheme or a U-ALE scheme is a matter of personal preference or implementational convenience.

(3) In ALE applications with large strains *and a dissipative material behaviour*, incremental formats arise in the constitutive update. Thus, convective terms appear in any case [19,20].

In the present study, whereby attention is focused on the application to hyperelasticity, use has been made of a T-ALE scheme, so that the presentation and implementation of the governing equations is not blurred by convective terms. Moreover, the proposed method contains the mesh-design independently of the user, whereby energy minimisation is the ultimate goal.

2.3. Monolithic ALE versus staggered ALE

In an ALE context, two sets of equations have to be solved, namely the considered equations of Newtonian mechanics (such as equilibrium, for instance) and the mesh motion. These equations are coupled: the respective unknowns (e.g. material displacements and nodal displacements, although also other options are possible) appear in both sets of equations. Formally, this suggests that the two sets of equations could be solved simultaneously. However, since this leads to an increased system of equations compared to the purely Lagrangian and purely Eulerian case, it has also been proposed to solve the two sets in a decoupled manner. In the sequel, distinction is made between Monolithic ALE schemes (M-ALE) in which the equations of Newtonian mechanics and mesh motion are solved simultaneously, i.e. coupled, and Staggered ALE schemes (S-ALE) in which the two sets of equations are solved alternatingly, i.e. uncoupled.

A disadvantage of M-ALE schemes is that they lead to larger matrices than S-ALE schemes. However, upon a proper linearisation, quadratic convergence of the Newton–Raphson solution algorithm can be maintained (see for instance Section 5.1). The reduction of number of iterations may balance the increase of computer cost per iteration.

Several strategies exist to formulate S-ALE schemes. In solid mechanics, it is common to distinguish within a S-ALE scheme between a purely Lagrangian substep and a purely Eulerian substep in the sense of an operator split. In the Lagrangian substep, mesh motion is neglected and the usual (Lagrangian) equations of mechanics are solved. The Eulerian substep serves to determine the mesh motion and to account for the convective terms. The more accurate option within a time step is to first carry out a Lagrangian substep followed by a Eulerian substep [29]. Next, it must be decided whether the Eulerian substep is carried out after every iteration (as in [17], for instance) or at the end of the time step (cf. Ref. [30], e.g.), see also [21,22,31] for comparisons (in Ref. [21], the term 'Updated ALE' is used to denote that a Eulerian substep is taken at the end of the time step). If a Eulerian substep is performed after every iteration, quadratic convergence is lost in the Newton–Raphson scheme of the Lagrangian substep. Nevertheless, equilibrium is fulfilled at the end of the time step. The inverse holds when a Eulerian substep is taken at the end of the time step: quadratic convergence within the Lagrangian substep and (possible) violation of equilibrium at the end of the time step are observed. However, it has been found that this possible unbalance at the end of the time step (i) is relatively small, and (ii) can be considered as an additional residual in the next time step, in which iterative corrections can be performed [22,31].

Another issue in discussing the efficiency of S-ALE schemes concerns the computational costs involved with a Eulerian (convective) substep. Nowadays, many low-cost, accurate convective schemes exist [22,23,29,30,32,33], therefore this is not considered to be a decisive issue.

In Section 4.2, both a M-ALE and a S-ALE scheme will be formulated. Comparisons are carried out in Section 5.

2.4. Remeshing strategies

As has been mentioned in Section 2.3, within an ALE formulation, two sets of equations have to be solved. Whereas the first set of equations is dictated by Newtonian mechanics, the second set of equations serves to improve the mesh quality, hence it is frequently referred to as the *remeshing strategy*. Within traditional ALE applications, the improvement of mesh quality has concentrated mainly on two aspects, namely mesh smoothing and mesh densification:

- Mesh smoothing is related to improving element shapes (i.e. avoiding element entanglement). This has been of primary concern in case of large deformations of the material, where Lagrangian analyses failed [15,17–20,22,30].
- Mesh densification is related to improving the resolution of the spatial discretisation in zones of special interest. Since in an ALE formulation the number of degrees of freedom and the element connectivity are constant throughout the computation, adapting the mesh implies that in certain parts of the domain the number of nodes (elements) is increased, whereas in other parts the number of nodes (elements) is decreased. The zones of special interest may include zones where the inelastic activity concentrates, or where steep gradients of the state variables occur [23–28,34,35]. In this paper, zones of special interest are those regions where inhomogeneities due to an inappropriate discretisation appear.

Implementation-wise, mesh smoothing and mesh densification are often treated as follows.

- For mesh smoothing, taylor-made strategies exist whereby normally the nodal displacements on the boundaries are prescribed and the nodal displacements in the domain are interpolated from the values at the boundaries [15,18,19,22]. Alternatively, Gauss–Seidel or Jacobi iterations can be used, in which element geometries are improved by shifting the nodes consecutively to optimal positions [36].
- Mesh densification can be achieved by defining a weight function that takes large values where small elements are desired and vice versa. The weight function can then be translated into the desired mesh motion in two ways: via Gauss/Seidel or Jacobi iterations, or via solving a partial differential equation. In the former approach, nodes are moved by considering the distribution of the weight function on a small patch of elements. This procedure is repeated for every node until convergence is obtained [34,35]. Another option is to include the weight function into a functional that is to be minimised, resulting in a partial differential equation with the nodal displacements as the fundamental unknowns [20,24,26–28].

Remark 2 (*ALE boundary conditions*). The ALE remeshing strategy has to be augmented with the corresponding boundary conditions. It is required that the boundary of the material domain and the boundary of the reference domain coincide throughout the analysis. Thus, material displacement of the boundary nodes in the normal direction is prohibited [15,20]. It is emphasised that the corresponding boundary integrals appear naturally when the remeshing strategy consists of solving a partial differential equation [12], so that enforcing the boundary conditions is straightforwardly achieved by setting these integrals to zero.

Remark 3 (*Remeshing*). Remeshing via a partial differential equation takes different formats for T-ALE schemes and for U-ALE schemes. In Ref. [28] these differences are treated in detail.

So far, the combination of mesh smoothing and mesh densification does not seem to be straightforward. Moreover, mesh densification often requires one or more user-defined parameters, which blurs the comparison between various remeshing strategies.

However, in the evaluation of different strategies it must be realised that at the very heart of (displacement-based) finite element methods lies the minimisation of potential energy—optimal meshes are therefore those meshes that lead to the lowest possible value for the potential energy. This is the main motivation for the present approach, which therefore completely circumvents the above-mentioned difficulties related to smoothing and densification.

3. Discrete governing equations

In the first part of this contribution, a dual equilibrium problem has been formulated in terms of spatial and material forces, whereby the fundamental unknowns of the two sets of equations are the spatial *and* the material placements of the nodes. As such, the dual equilibrium problem is intrinsically an ALE formulation. The spatial motion problem (i.e. the equilibrium of spatial forces, or the direct motion problem) can be considered as the Lagrangian equations that are commonly solved in solid mechanics. On the other hand, the material motion problem (i.e. the equilibrium of material forces, or the inverse motion problem) then serves as the Eulerian counterpart, including the remeshing strategy. It is emphasised that the two equations are presented according to the monolithic algorithm (see Section 2.3), and that the remeshing strategy is derived from minimisation of potential energy.

The dual equilibrium problem can be written in many different formats, including different configurations. In Part 1 of this contribution, the discretisation and linearisation of the general dual equilibrium problem have been derived. In the spirit of Eqs. (44)–(46) of Part 1, the discretised residuals of the coupled problem read

$$\begin{aligned}
\mathbf{R}^I_{\bar{\varphi}} &= \mathop{\mathbf{A}}_{e=1}^{n_{\mathrm{el}}} \int_{\mathscr{B}^e_t} \nabla_{\boldsymbol{x}} N^i_{\bar{\varphi}} \cdot \boldsymbol{\sigma} \,\mathrm{d}V_t - \int_{\partial\mathscr{B}^{te}_t} N^i_{\bar{\varphi}} \boldsymbol{t}_t \,\mathrm{d}A_t - \int_{\mathscr{B}^e_t} N^i_{\bar{\varphi}} \boldsymbol{b}_t \,\mathrm{d}V_t = \mathbf{0}, \\
\mathbf{R}^J_{\tilde{\Phi}} &= \mathop{\mathbf{A}}_{e=1}^{n_{\mathrm{el}}} \int_{\mathscr{B}^e_0} \nabla_{\boldsymbol{X}} N^j_{\tilde{\Phi}} \cdot \boldsymbol{\Sigma} \,\mathrm{d}V_0 - \int_{\partial\mathscr{B}^{te}_0} N^j_{\tilde{\Phi}} \boldsymbol{T}_0 \,\mathrm{d}A_0 - \int_{\mathscr{B}^e_0} N^j_{\tilde{\Phi}} \boldsymbol{B}_0 \,\mathrm{d}V_0 = \mathbf{0}.
\end{aligned} \tag{2}$$

where $\mathbf{A}_{e=1}^{n_{\mathrm{el}}}$ implies an assembly over all elements and n_{el} is the number of elements. Moreover, $N^i_{\bar{\varphi}}$ and $N^j_{\tilde{\Phi}}$ denote the shape functions used for the spatial motion problem and the material motion problem. The body forces and the traction forces of the spatial and the material motion problem are denoted as $\boldsymbol{b}_t$, $\boldsymbol{B}_0$, $\boldsymbol{t}_t$ and $\boldsymbol{T}_0$, respectively. The corresponding linearisation defines the following entries of the tangent stiffness matrix,

$$\begin{aligned}
\mathbf{K}^{IK}_{\bar{\varphi}\bar{\varphi}} &= \mathop{\mathbf{A}}_{e=1}^{n_{\mathrm{el}}} \int_{\mathscr{B}^e_0} \nabla_{\boldsymbol{x}} N^i_{\bar{\varphi}} \cdot \mathbf{c} \cdot \nabla_{\boldsymbol{x}} N^k_{\bar{\varphi}} \,\mathrm{d}V_0, \\
\mathbf{K}^{IL}_{\bar{\varphi}\tilde{\Phi}} &= \mathop{\mathbf{A}}_{e=1}^{n_{\mathrm{el}}} \int_{\mathscr{B}^e_t} \nabla_{\boldsymbol{x}} N^i_{\bar{\varphi}} \cdot \mathrm{d}_{\boldsymbol{f}}\boldsymbol{\sigma}^t \cdot \boldsymbol{f}^t \cdot \nabla_{\boldsymbol{X}} N^l_{\tilde{\Phi}} \,\mathrm{d}V_t - \int_{\mathscr{B}^e_t} N^i_{\bar{\varphi}} \boldsymbol{b}_t \cdot \nabla_{\boldsymbol{X}} N^l_{\tilde{\Phi}} \,\mathrm{d}V_t, \\
\mathbf{K}^{JK}_{\tilde{\Phi}\bar{\varphi}} &= \mathop{\mathbf{A}}_{e=1}^{n_{\mathrm{el}}} \int_{\mathscr{B}^e_0} \nabla_{\boldsymbol{X}} N^j_{\tilde{\Phi}} \cdot \mathrm{D}_{\boldsymbol{F}}\boldsymbol{\Sigma}^t \cdot \boldsymbol{F}^t \cdot \nabla_{\boldsymbol{x}} N^k_{\bar{\varphi}} \,\mathrm{d}V_0 - \int_{\mathscr{B}^e_0} \nabla_{\boldsymbol{X}} N^j_{\tilde{\Phi}} \cdot \boldsymbol{b}_0 N^k_{\bar{\varphi}} \,\mathrm{d}V_0, \\
\mathbf{K}^{JL}_{\tilde{\Phi}\tilde{\Phi}} &= \mathop{\mathbf{A}}_{e=1}^{n_{\mathrm{el}}} \int_{\mathscr{B}^e_t} \nabla_{\boldsymbol{X}} N^j_{\tilde{\Phi}} \cdot \mathbf{C} \cdot \nabla_{\boldsymbol{X}} N^l_{\tilde{\Phi}} \,\mathrm{d}V_t,
\end{aligned} \tag{3}$$

whereby $\boldsymbol{b}_0 = J\boldsymbol{b}_t$, while the fourth order tensors $\mathbf{c}$, $\mathrm{D}_{\boldsymbol{F}}\boldsymbol{\Sigma}^t \cdot \boldsymbol{F}^t$, $\mathrm{d}_{\boldsymbol{f}}\boldsymbol{\sigma}^t \cdot \boldsymbol{f}^t$ and $\mathbf{C}$ will be explained in the sequel. After the assembly the global system of linearised equations can formally be written as

$$\begin{bmatrix} \mathbf{K}_{\bar{\varphi}\bar{\varphi}} & \mathbf{K}_{\bar{\varphi}\tilde{\Phi}} \\ \mathbf{K}_{\tilde{\Phi}\bar{\varphi}} & \mathbf{K}_{\tilde{\Phi}\tilde{\Phi}} \end{bmatrix} \begin{bmatrix} \Delta\bar{\boldsymbol{\varphi}} \\ \Delta\tilde{\boldsymbol{\Phi}} \end{bmatrix} = - \begin{bmatrix} \mathbf{R}_{\bar{\varphi}} \\ \mathbf{R}_{\tilde{\Phi}} \end{bmatrix}, \tag{4}$$

where the first line of equations denotes the linearisation of the spatial motion problem and the second line refers to the linearisation of the material motion problem. The global vector of unknowns $\bar{\boldsymbol{\varphi}}$ and $\tilde{\boldsymbol{\Phi}}$ designates the spatial and material placements of the nodes, respectively. The various stress measures and material tangent stiffness relations are given for the general hyperelastic case in Part 1 of this contribution, and for the special Neo–Hookean case below.

Remark 4 (*Linearisation of body forces*). Since the nodes are allowed to move with respect to the material, the volumes of the elements will change. This has an influence on the equivalent nodal forces that are associated with the body force, and this influence is accounted for by the body force contributions in expressions (3_2) and (3_3).

Next, the specialisation to hyperelasticity of the compressible Neo–Hookean type is made, whereby, for the sake of clarity, we neglect contributions from the external potential energy density V_0. The internal potential energy density W_0 in the material configuration is written as

$$W_0 = \tfrac{1}{2}\lambda_0 \ln^2 J + \tfrac{1}{2}\mu_0[\boldsymbol{I} : \boldsymbol{C} - n^{\dim} - 2\ln J], \tag{5}$$

where λ_0 and μ_0 are the usual Lamé constants, $n^{\dim}$ is the number of spatial dimensions of the problem, $J = \det \boldsymbol{F}$, $\boldsymbol{C} = \boldsymbol{F}^t \cdot \boldsymbol{F}$ is the right Cauchy–Green strain tensor, and $\boldsymbol{F} = \nabla_{\boldsymbol{X}} \boldsymbol{\varphi}$ is the spatial motion deformation gradient.

This allows to express the stress quantities and material tangents that appear in Eqs. (2) and (3) explicitly as functions of the deformation gradient. In particular,

$$\boldsymbol{\sigma}^t = [\lambda_t \ln J - \mu_t]\boldsymbol{I} + \mu_t \boldsymbol{b}, \tag{6}$$

$$\boldsymbol{\Sigma}^t = \left[\frac{1}{2}\lambda_0 \ln J[\ln J - 2] + \frac{1}{2}\mu_0[\boldsymbol{I} : \boldsymbol{C} + 2 - n^{\dim} - 2\ln J]\right]\boldsymbol{I} - \mu_0 \boldsymbol{C} \tag{7}$$

for the stresses that appear in the right-hand-side residuals, and

$$\mathsf{c} = \lambda_0 \boldsymbol{I} \otimes \boldsymbol{I} - [\lambda_0 \ln J - \mu_0]\boldsymbol{I} \underline{\otimes} \boldsymbol{I} + \mu_0 \boldsymbol{I} \overline{\otimes} \boldsymbol{b}, \tag{8}$$

$$\mathrm{d}_{\boldsymbol{f}}\boldsymbol{\sigma}^t \cdot \boldsymbol{f}^t = [\lambda_t[\ln J - 1] - \mu_t]\boldsymbol{I} \otimes \boldsymbol{I} + \mu_t[\boldsymbol{b} \otimes \boldsymbol{I} - \boldsymbol{F} \underline{\otimes} \boldsymbol{F} - \boldsymbol{F} \overline{\otimes} \boldsymbol{F}], \tag{9}$$

$$\mathrm{D}_{\boldsymbol{F}}\boldsymbol{\Sigma}^t \cdot \boldsymbol{F}^t = [\lambda_0[\ln J - 1] - \mu_0]\boldsymbol{I} \otimes \boldsymbol{I} + \mu_0[\boldsymbol{I} \otimes \boldsymbol{b} - \boldsymbol{F}^t \underline{\otimes} \boldsymbol{F}^t - \boldsymbol{F}^t \overline{\otimes} \boldsymbol{F}^t], \tag{10}$$

$$\begin{aligned}\mathsf{C} = {} & \left[\lambda_t\left[\frac{1}{2}\ln^2 J - 2\ln J + 1\right] + \frac{1}{2}\mu_t[\boldsymbol{I} : \boldsymbol{C} + 4 - n^{\dim} - 2\ln J]\right]\boldsymbol{I} \otimes \boldsymbol{I} \\ & + \left[\lambda_t\left[-\frac{1}{2}\ln^2 J + \ln J\right] + \frac{1}{2}\mu_t[-\boldsymbol{I} : \boldsymbol{C} + 2 - n^{\dim} + 2\ln J]\right]\boldsymbol{I} \underline{\otimes} \boldsymbol{I} \\ & + \mu_t[\boldsymbol{C} \overline{\otimes} \boldsymbol{I} + \boldsymbol{C} \underline{\otimes} \boldsymbol{I} + \boldsymbol{I} \underline{\otimes} \boldsymbol{C} - \boldsymbol{C} \otimes \boldsymbol{I} - \boldsymbol{I} \otimes \boldsymbol{C}]\end{aligned} \tag{11}$$

for the relevant tangents. In the above relations, $\boldsymbol{b} = \boldsymbol{F}^t \cdot \boldsymbol{F}$ is the left Cauchy–Green strain tensor.

Remark 5 (*Symmetry*). By means of Eqs. (9) and (10) it can be verified that the coupled system given in expression (4) is symmetric—note that expressions (3_2) and (3_3) are evaluated on the spatial configuration $\mathscr{B}_t$ and the material configuration $\mathscr{B}_0$, respectively.

4. Implementational aspects

The finite element matrix-vector equations are importantly simplified in case of a one-dimensional problem, therefore the one-dimensional discrete system is treated separately in Section 4.1. A general multi-dimensional M-ALE scheme and a S-ALE scheme are formulated in Section 4.2. Furthermore, two issues are discussed that are specific for the material motion problem, namely the treatment of a possible singular stiffness in the dual equilibrium problem (Section 4.3) and the incrementation of the material force residual (Section 4.4).

4.1. One-dimensional implementation

For the one-dimensional case, we set $\lambda_0 = 0$ and $\mu_0 = \frac{1}{2}E$. Thus the internal and external potential energy density W_0 and V_0 simplify to

$$W_0 = \tfrac{1}{4}E[F^2 - 1 - 2\ln J] \quad V_0 = -b_0\varphi, \tag{12}$$

whereby b_0 is assumed to be constant, $b_0 = \text{const}$. Moreover, important simplifications apply, most notably the fact that $J = \det F = F$ and $j = \det f = f$. The Cauchy stress σ and the Eshelby stress Σ thus specialise as

$$\sigma = \frac{1}{2}E\left[\frac{\overline{F}}{\tilde{f}} - \frac{\tilde{f}}{\overline{F}}\right], \tag{13}$$

$$\Sigma = \frac{1}{4}E\left[-\frac{\overline{F}^2}{\tilde{f}^2} + 1 - 2\ln\frac{\overline{F}}{\tilde{f}}\right] - b_0\left[\bar{\varphi}\circ\tilde{\Phi}^{-1}\right], \tag{14}$$

whereby we have expressed the spatial motion deformation gradient F and the material motion deformation gradient f in terms of the referential gradients $\tilde{f}$ and $\overline{F}$ as $F = \overline{F}/\tilde{f}$ and $f = \tilde{f}/\overline{F}$ and the spatial motion map φ as the composition of mappings $\varphi = \bar{\varphi}\circ\tilde{\Phi}^{-1}$. When pulling back all the integrals to the one-dimensional reference configuration $l_\square$, we can express the corresponding residuals in the following form.

$$\mathsf{R}^I_{\bar{\varphi}} = \mathop{\mathsf{A}}_{e=1}^{n_{\text{el}}}\int_{l^e_\square}\nabla_\xi N^i_{\bar{\varphi}}\sigma\,\mathrm{d}l_\square - \int_{l^e_\square}N^i_{\bar{\varphi}}b_\square\,\mathrm{d}l_\square - \int_{\partial l^e_\square}N^i_{\bar{\varphi}}t_\square\,\mathrm{d}\partial l_\square, \tag{15}$$

$$\mathsf{R}^J_{\tilde{\Phi}} = \mathop{\mathsf{A}}_{e=1}^{n_{\text{el}}}\int_{l^e_\square}\nabla_\xi N^j_{\tilde{\Phi}}\Sigma\,\mathrm{d}l_\square - \int_{l^e_\square}N^j_{\tilde{\Phi}}B_\square\,\mathrm{d}l_\square - \int_{\partial l^e_\square}N^j_{\tilde{\Phi}}T_\square\,\mathrm{d}\partial l_\square. \tag{16}$$

Thus, the tangent stiffness contributions given in (3) specialises as follows:

$$\mathsf{K}^{IK}_{\bar{\varphi}\bar{\varphi}} = \mathop{\mathsf{A}}_{e=1}^{n_{\text{el}}}\int_{l^e_\square}\nabla_\xi N^i_{\bar{\varphi}}\frac{E}{2}\left[\frac{1}{\tilde{f}} + \frac{\tilde{f}}{\overline{F}^2}\right]\nabla_\xi N^k_{\bar{\varphi}}\,\mathrm{d}l_\square, \tag{17}$$

$$\mathsf{K}^{IL}_{\bar{\varphi}\tilde{\Phi}} = \mathop{\mathsf{A}}_{e=1}^{n_{\text{el}}} - \int_{l^e_\square}\nabla_\xi N^i_{\bar{\varphi}}\frac{E}{2}\left[\frac{\overline{F}}{\tilde{f}^2} + \frac{1}{\overline{F}}\right]\nabla_\xi N^l_{\tilde{\Phi}}\mathrm{d}l_\square - \int_{l^e_\square}N^i_{\bar{\varphi}}b_0\nabla_\xi N^l_{\tilde{\Phi}}\,\mathrm{d}l_\square, \tag{18}$$

$$\mathsf{K}^{JK}_{\tilde{\Phi}\bar{\varphi}} = \mathop{\mathsf{A}}_{e=1}^{n_{\text{el}}} - \int_{l^e_\square}\nabla_\xi N^j_{\tilde{\Phi}}\frac{E}{2}\left[\frac{\overline{F}}{\tilde{f}^2} + \frac{1}{\overline{F}}\right]\nabla_\xi N^k_{\bar{\varphi}}\,\mathrm{d}l_\square - \int_{l^e_\square}\nabla_\xi N^j_{\tilde{\Phi}}b_0N^k_{\bar{\varphi}}\,\mathrm{d}l_\square, \tag{19}$$

$$\mathsf{K}^{JL}_{\tilde{\Phi}\bar{\Phi}} = \mathop{\mathbf{A}}_{e=1}^{n_{\mathrm{el}}} \int_{l^e_\square} \nabla_\xi N^j_{\tilde{\Phi}} \frac{E}{2} \left[\frac{1}{\bar{f}} + \frac{\overline{F}^2}{\bar{f}^3} \right] \nabla_\xi N^l_{\bar{\Phi}} \, \mathrm{d}l_\square. \tag{20}$$

Note the symmetry of system, since $\mathsf{K}^{IL}_{\bar{\varphi}\tilde{\Phi}} = \mathsf{K}^{LI}_{\tilde{\Phi}\bar{\varphi}}$.

4.2. Formulation of M-ALE and S-ALE schemes

A monolithic ALE (M-ALE) solution scheme takes into full account the coupling that exists between the spatial motion problem and the material motion problem. Hence, no further simplifications of the system of equations as shown in expression (4) are made.

Alternatively, the spatial motion problem and the material motion problem can be solved in an alternating manner. As such, a staggered (S-ALE) or decoupled solution scheme is obtained. This is accomplished by neglecting the off-diagonal parts of the stiffness matrix, i.e. setting $\mathbf{K}_{\bar{\varphi}\tilde{\Phi}}$ and $\mathbf{K}_{\tilde{\Phi}\bar{\varphi}}$ of Eq. (4) equal to zero. Thus, the spatial motion problem serves to compute the spatial coordinates of the nodes, whereas the material motion problem is used to calculate the material coordinates of the nodes (i.e. the material motion problem provides the remeshing strategy). A load step is subdivided into several substeps, in which the spatial motion problem and the material motion problem are solved successively. To invoke the emergence of non-zero material force residuals, it is required to start with the spatial motion problem (see the argument provided in Section 4.3). Furthermore, since mesh optimisation is of little value when no subsequent substep in the spatial motion problem is taken, the final substep consists of only solving the spatial motion problem. Both the spatial motion problem and the material motion problem are solved iteratively until convergence of the corresponding unknowns (spatial coordinates of the nodes and material coordinates of the nodes, respectively) is obtained. In short, if a load increment is subdivided into n substeps (n being a positive integer), the spatial motion problem is solved n times and the material motion problem $n-1$ times. Taking $n = 1$ leads to a purely Lagrangian approach.

4.3. Dynamic constraints

Special treatment is needed for nodes with vanishing material force residual. In that case, a singularity in the system of equations exists. This can be understood as follows: since material forces are associated with a variation $\delta\tilde{\boldsymbol{\Phi}}$ at fixed x, a zero material residual force implies that infinitely large variations $\delta\tilde{\boldsymbol{\Phi}}$ would be admissible. This corresponds to a singular stiffness in the dual equilibrium problem. To avoid this, nodes with zero material force residual have to be constrained. This may seem an important restriction. However, as shown by Mueller and Maugin [9] and below in Section 5, the case of zero material force residual for a certain node corresponds with an *optimal material position* for that node, therefore nodes with zero material force residual *do not need* improvement of their material position.

The situation that one or more nodes have zero material force residual can occur at various instants during the computation. At least at the beginning of every increment the material force residual of every internal node is zero (provided that a converged solution has been found for the previous increment and, hence, a residual within the convergence tolerance has been obtained). In subsequent iterations, the nodal position may not be optimal any longer and a non-zero material force may emerge. Hence, the additional constraints have to be imposed selectively: a *dynamic constraint imposition* is required. This can be achieved in various ways:

- on the structural (global) level, constraints can be activated and de-activated on the global level, such that the number of equations that is solved for can change from iteration to iteration;

- on the element (local) level, the material motion part of the stiffness matrix can temporarily be substituted by a unit matrix in case a constraint needs to be imposed. The off-diagonal parts of the stiffness matrix (i.e. the parts relating the spatial motion problem to the material motion problem for the degree of freedom under consideration) should then be set to zero, and the corresponding terms in the right-hand-side vector should be set equal to the current material coordinates.

4.4. Initialisation

The driving forces of the spatial motion problem and the material motion problem are the spatial (or physical) forces and the material (or configurational) forces, respectively. Whereas a residual of spatial forces is an indication of spatial equilibrium, a residual of material forces gives an indication of material equilibrium, that is, of material homogeneity [2].

The convergence radius of the Newton–Raphson scheme is restricted to solution vectors sufficiently close to the exact solution. For the spatial motion problem in solid mechanics, this has motivated the use of load incrementation. That is, the (spatial) load is applied not at once, but in a number of small steps. For small enough load steps, within each load step the spatial forces residual is sufficiently small, and convergence of the Newton–Raphson scheme can be expected.

Also the Newton–Raphson convergence radius for the material motion problem is restricted. However, the driving force behind the material motion problem, namely discrete material forces, cannot be incremented in an as straightforward manner as in the spatial motion problem. As is further explained in Remark 7, subincrementing the applied load does *not* lead to subincrementation of the material forces. Thus, a sophisticated strategy must be devised.

It is emphasised that a proper incrementation of the material motion problem only poses a problem at the start of the analysis: once the material coordinates have adopted optimal values for the first load step, it can be expected that these material coordinates will also be more or less optimal for subsequent load steps. Thus, convergence problems are not expected after the first load step. A solution strategy for the first step could be to use a staggered scheme in the following manner:

(1) The spatial motion problem is solved.
(2) The discrete residual of the material forces are computed node-wise.
(3) This discrete material residual can be applied in a number of increments in order to solve the material motion problem.
(4) As soon as material coordinates have been obtained that are reasonably close to optimal, the system can be solved again in a monolithic manner, if desired.

Another option would be to include line-search techniques, so that divergence of the Newton–Raphson procedure is circumvented. However, more study is needed for a better understanding of the incrementation of material forces in the material motion problem.

5. Examples

The various concepts are first illustrated by means of a one-dimensional example. Then, two-dimensional examples are treated. Throughout, linear finite elements have been used: two-noded elements in 1D and four-noded quadrilaterals in 2D. For the two-dimensional examples only M-ALE solutions are considered which have been denoted simply as ALE solutions.

5.1. Uni-axial bar

As a first example, a one-dimensional bar with length 10 mm clamped at both ends is considered. A uniform body load $b_0 = 100$ N/mm is taken, and Young's modulus $E = 1000$ MPa. The coordinate axis has its origin at the left end of the bar, see also Fig. 2.

Firstly, a pure Lagrangian setting of the problem is studied, i.e. no mesh motion is permitted and the material motion problem is not taken into account. Two linear finite elements have been used to discretise the bar; since the outer nodes are fixed, the only degree of freedom of the system concerns with the central node. The goal of this extremely simplified analysis is to investigate the potential energy as a function of the location of the central node (simply denoted as X) and its displacement (denoted as u).

In Fig. 3, a contour plot of the potential energy as a function of X and u is shown. Obviously, for a certain value of X the finite element solution would predict a displacement u that minimises the potential energy *for that given value of X* (that is, the potential energy is minimised along a vertical cross section of the contour plot). These values of u are indicated by the dashed line. Only for one value of X a *global* minimum of the potential energy is obtained; in the present case this absolute minimum corresponds to $X = 4.5868$ mm and $u = 1.2290$ mm, denoted by a star in the contour plot. Due to the non-symmetry of the

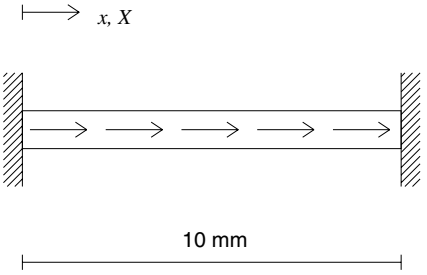

Fig. 2. Bar—problem statement.

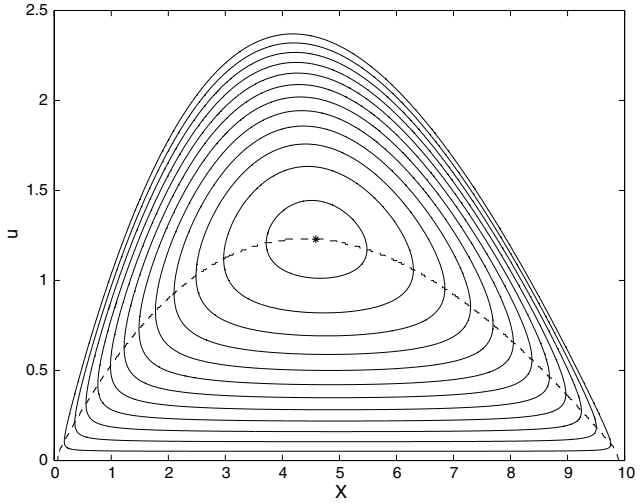

Fig. 3. Bar, Lagrangian analysis—contour plots of potential energy as a function of the midnode position X and the midnode displacement u.

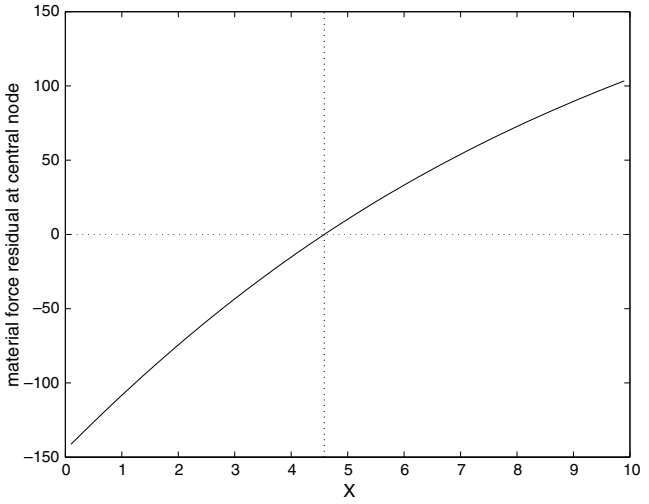

Fig. 4. Bar, Lagrangian analysis—residual material force at central node versus material coordinate of central node.

Neo–Hookean strain energy function in tension and compression, the absolute minimum renders a material coordinate X which is not situated right in the middle of the bar but is shifted slightly to the left.

The relation between the position of the central node and the resulting residual material force at that node is shown in Fig. 4. For non-optimal values of X, that is if $X \neq 4.5868$, a non-zero residual material force emerges. Furthermore, if the central node is positioned *left* of its optimal position a *negative* material force is found, and vice versa. Thus, a mesh is optimised by moving the nodes in the direction *opposite* to the nodal material forces residual, which corresponds to a release of energy.

Within an ALE setting of the previous problem statement, the central node is admitted to move with respect to the material. Firstly, the M-ALE scheme is taken, and three initial positions of the central node have been tested: $X = 5$ mm, $X = 7$ mm and $X = 9$ mm within a single load step. In Fig. 5 the behaviour of the three solutions during the iterative process is shown. The different line segments connect the solutions found in successive iterations. (Notice that all three solutions start with a vertical line segment, which is due to the fact that the material motion problem is neglected in the first iteration—see Section 4.3.) Independent of the initial position that is assigned to the central node, the scheme converges towards the solution $X = 4.5868$ mm and $x - X = 1.2290$ mm as predicted by the Lagrangian analysis above. Thus, the ALE scheme leads to a potential energy that is minimum in a global sense. The convergence behaviour of the M-ALE scheme for different initial positions of the central node is also shown in Fig. 6. The residual is measured in terms of the norm of the right-hand-side vector, normalised with the value at the beginning of the increment. As can be seen, the convergence is asymptotically quadratic for all three analyses. However, only for $X = 5$ mm initially the convergence is monotonic; taking an initially (strongly) inhomogeneous mesh via $X = 7$ mm or $X = 9$ mm leads to a temporary increase of the residual in the third iteration (although it must be noted that this is only the second iteration for the material motion problem, since in the first iteration only the spatial motion problem is solved—cf. Section 4.3). This would advocate the use of meshes that are initially homogeneous. Since it is normally dictated by the mechanical response of the system to take small load steps, it is expected that the mesh requirements will not change much from increment to increment. Starting from a condition of no loading, a uniform mesh is optimal, after which the mesh can be adapted gradually according to the loading state.

In Fig. 7 the nodal displacement versus material coordinate is plotted for various meshes (consisting of 2, 4, 8 and 16 elements) using the M-ALE scheme. As can be verified, convergence upon mesh refinement is

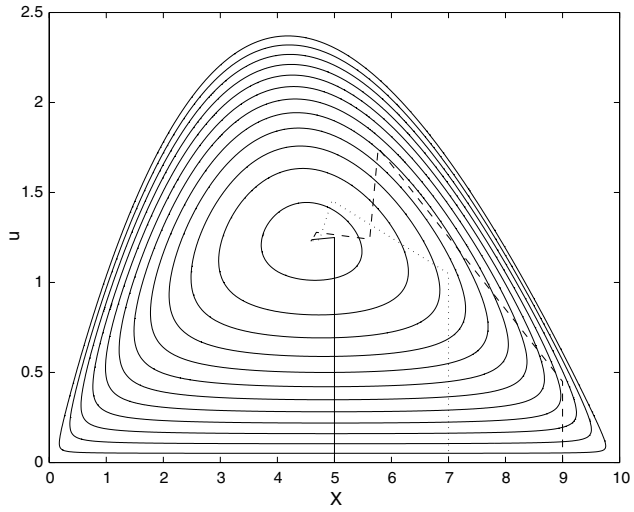

Fig. 5. Bar, M-ALE analysis—contour plots of potential energy and convergence behaviour of M-ALE scheme for initial midnode position $X = 5$ (solid), $X = 7$ (dotted) and $X = 9$ (dashed).

obtained. It is emphasised that both the direct motion problem and the inverse motion problem are *displacement methods* (as opposed to force methods or hybrid methods), therefore upon mesh refinement a monotonic convergence is expected in which the exact potential energy is approximated from above. This is shown in Fig. 8, in which the convergence of the potential energy upon mesh refinement is plotted in a double logarithmic scale. In this graph, the relative error in the potential energy is normalised with the potential energy obtained with a very fine Lagrangian mesh.

Finally, a comparison is made between the M-ALE scheme and the S-ALE scheme. As has been argued and shown above, the M-ALE scheme leads to meshes that have a global minimum of potential energy. An

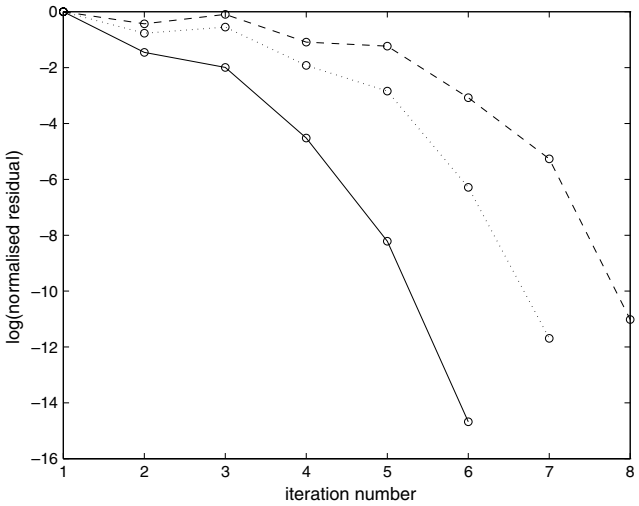

Fig. 6. Bar, M-ALE analysis—convergence behaviour depending on initial position X of midnode: $X = 5$ (solid), $X = 7$ (dotted) and $X = 9$ (dashed).

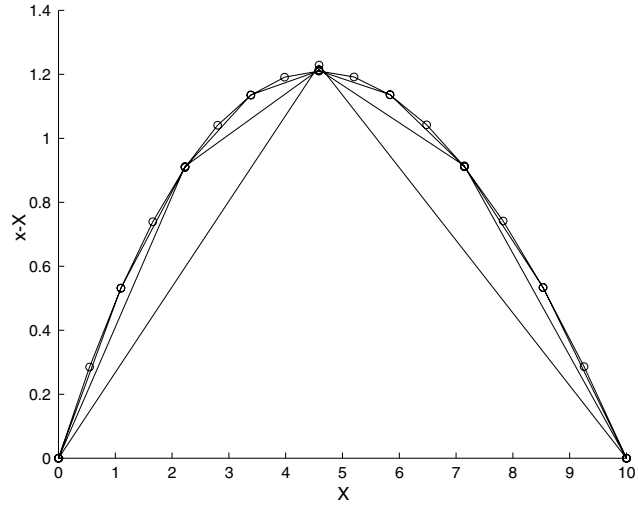

Fig. 7. Bar, M-ALE analysis—nodal displacement $x - X$ versus material coordinate X for meshes of 2, 4, 8 and 16 elements.

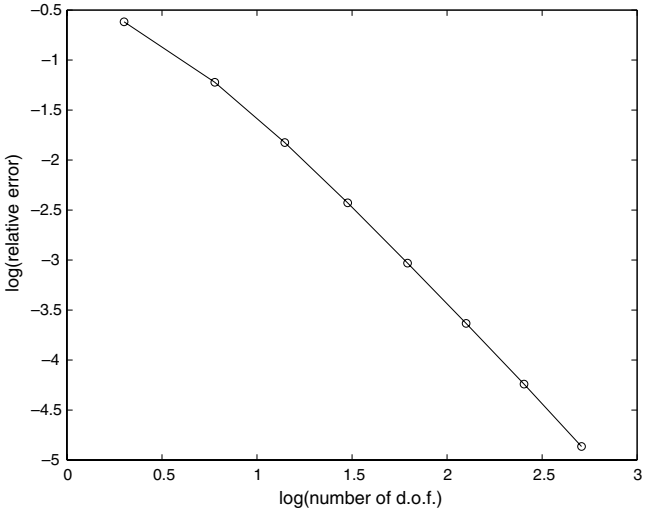

Fig. 8. Bar, M-ALE analysis—relative error in potential energy versus number of degrees of freedom.

obvious question would then be, to what extent do the M-ALE scheme and the S-ALE scheme coincide; or, since the M-ALE can be considered as the exact solution of the *discretised problem*, to what extent is the S-ALE scheme capable of matching the performance of the M-ALE scheme. As will be shown below, this strongly depends on the number of substeps that is taken. The S-ALE scheme consists of n spatial motion steps and $n - 1$ material motion steps, where n is the number of substeps. Obviously, the larger the number of substeps, the more mutual interference is enabled between the spatial motion problem and the material motion problem. This dependence on the number of substeps is absent in the M-ALE scheme.

In Fig. 9 the performance of the M-ALE scheme and the S-ALE scheme are compared for the case of 2 finite elements, i.e. one interior node. On the horizontal axis the number of substeps is plotted in a

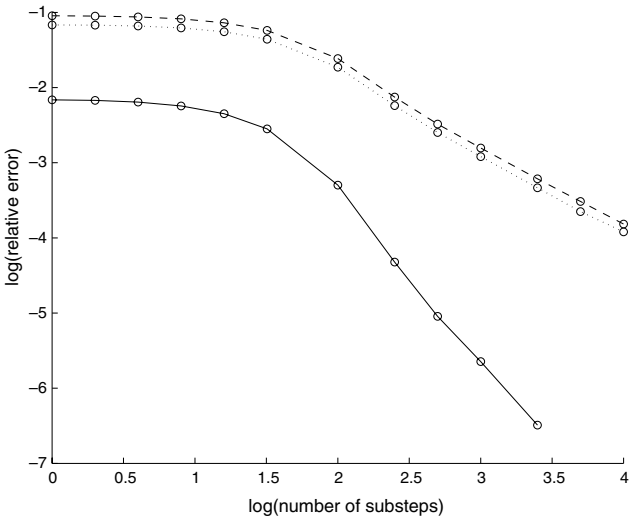

Fig. 9. Bar—performance of S-ALE scheme as compared to (exact) M-ALE scheme in terms of potential energy (solid), material coordinate X of central node (dotted) and spatial coordinate x of central node (dashed).

logarithmic scale (whereby it is noted that for n substeps the load is subdivided into n equal steps). On the vertical axis the difference between the M-ALE scheme and the S-ALE scheme is plotted in a logarithmic scale. For this difference, three quantities are investigated: the potential energy of the system, and the spatial and material coordinate of the central node. On the extreme left of the graph, i.e. $\log(n) = 0$, the S-ALE scheme simplifies to the pure Lagrangian case. If an improvement of the performance of the S-ALE scheme compared to the pure Lagrangian case is desired of, say, one significant digit (i.e. a difference of one unit on the vertical axis), then about 100 substeps (i.e. a difference of 2 units on the horizontal axis) are required. Afterwards, the accuracy of the potential energy increases with two digits when the number of substeps is increased by a factor 10, and that of the spatial and material coordinates with one digit for 10 times as many substeps.

The computational effort of the M-ALE scheme and the S-ALE scheme involve the assembly of one matrix of size $2N$ and two matrices of size N, respectively, where N is the number of nodes for the one-dimensional case. However, for comparable accuracies the number of load steps required for the S-ALE scheme is much higher than that of the M-ALE scheme. Unless problems with a very large number of degrees of freedom are considered, the M-ALE scheme is more efficient than the S-ALE scheme as presented here. A reason for this could be the strong coupling that exists between the two equations (the off-diagonal parts of the matrix in system (4) are of the same order of magnitude as the diagonal parts), so that decoupling leads to relatively large discrepancies. The study and/or development of more efficient staggered solution schemes is beyond the scope of the current work.

5.2. Homogeneous block under tension

The second example concerns with a homogeneous block under tension. The geometry and loading conditions are adopted from Ref. [9] and shown in Fig. 10. The elasticity constants are given as $E_0 = 200\,000$ MPa and $\nu_0 = 0.3$ (i.e. $\lambda_0 = 115\,385$ MPa and $\mu_0 = 76\,923$ MPa). The finite element discretisation consists of 4×4 elements. For the spatial motion problem, the horizontal displacement of upper and lower edge, which are subjected to tension, are constrained. The specimen is loaded by displacement

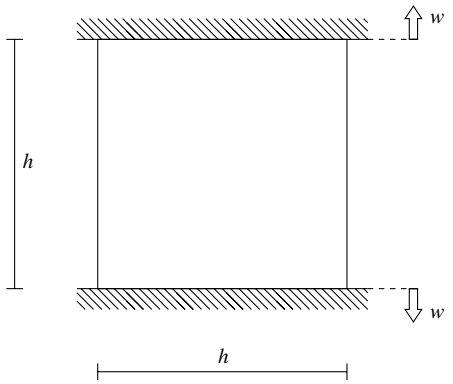

Fig. 10. Homogeneous block under tension—problem statement.

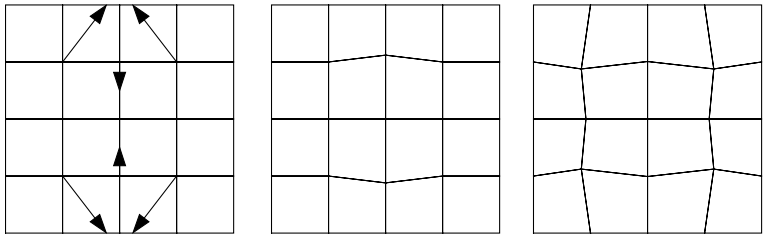

Fig. 11. Homogeneous block under tension—material domain $\mathscr{B}_0$ for zero (left), two (middle) and 12 (right) material degrees of freedom unconstrained; left picture includes discrete material forces for interior nodes.

increments $0.0025h$, up to a final displacement of $0.5h$. Different boundary conditions have been taken for the material motion problem, in correspondence with the cases studied in [9].

Firstly, keeping all nodes fixed a Lagrangian description is obtained that serves to calculate material forces, as is depicted in Fig. 11 (left). Only the material forces of interior nodes are plotted, which are in excellent qualitative agreement with Mueller and Maugin [9], whereas the total energy for this configuration is given as $\mathscr{I}^{\text{lagrange}} = 11.6724$ N mm.

Remark 6 (*Displaying material forces*). In Fig. 11 (left) the material forces of the boundary nodes are not plotted, in contrast to the associated figure in [9]. Boundaries can be considered as an extreme inhomogeneity, therefore they lead to material forces that differ an order of magnitude with material forces at interior nodes. Since it is aimed here to minimise the effects of inhomogeneities due to discretisation, material forces stemming from other inhomogeneities are not considered.

Secondly, only the second and fourth midnode on the vertical axis of symmetry are allowed to move, and only in the vertical direction (which corresponds to 2 degrees of freedom in the material motion problem). The resulting nodal coordinates in $\mathscr{B}_0$ are shown in Fig. 11, middle. The material displacement $\tilde{\Phi}$ of the considered second and fourth midnode is found as $0.0301h$, thus new vertical coordinates $0.2199h$ and $0.7801h$ are obtained, which again agree perfectly with the results of Mueller and Maugin [9]. For this set of boundary conditions, the total energy $\mathscr{I}^{\text{ale02}} = 11.6717$ N mm, which is somewhat below the value obtained with the purely Lagrangian analysis.

Table 1
Homogeneous block under tension—typical convergence of Newton–Raphson iterations

Iteration	Norm of residual	Total energy $\mathscr{I}^{\text{ale12}}$
0	1.58114E−02	0.0000000000E+00
1	3.92275E+00	1.1672534150E+01
2	1.24279E+01	1.1669273828E+01
3	1.27318E+00	1.1668864896E+01
4	1.85232E−02	1.1668859084E+01
5	5.75864E−06	1.1668859082E+01
6	6.31087E−11	1.1668859082E+01

Finally, all internal nodes are allowed to move (i.e. 12 degrees of freedom in the material motion problem), the resulting mesh of which is shown in Fig. 11 (right). For this case, the total energy $\mathscr{I}^{\text{ale12}} = 11.6688$ N mm, which is again lower than in the previous analysis. In short, $\mathscr{I}^{\text{ale12}} < \mathscr{I}^{\text{ale02}} < \mathscr{I}^{\text{lagrange}}$; that is, the more degrees of freedom are included in the material motion problem (or the more nodes are allowed to move), the more the total energy decreases. For a representative load step, the convergence of the Newton–Raphson iterations is illustrated in Table 1. As can be verified, a quadratic convergence towards an optimal mesh is obtained, which is an important improvement compared to the 500 iterations reported in [9] needed to obtain the optimal mesh.

Remark 7 (*Load-dependent optimal mesh*). It is important to note that, as prescribed displacements are increased, nodes tend to move back to their original position. Thus, the optimal node point position depends on the magnitude of the applied load (or, more precisely, on the degree of geometric non-linearity).

Remark 8 (*Singularities*). The ultimate ALE analysis of the homogeneous block under tension would be to allow the edge nodes to move tangentially to the edges, in addition to free movement of the interior nodes. However, in this example singularities arise at the vertices of the specimen, which have a deteriorating effect on the mesh optimisation process and on the convergence of the Newton–Raphson iterations. Therefore, this case is not considered here.

5.3. Homogeneous block under bending

Next, the same square, homogeneous block is subjected to bending. The same material parameters as in Section 5.2 are used, and for the geometry $h = 1$ mm is taken. For the discretisation, 8×8 elements are used. The boundary conditions of the spatial motion problem consist of prescribed displacements at vertical edges, whereas the left and right midheight node of each vertical edge are held fixed completely. For the material motion problem, nodes of all edges are constrained horizonally and vertically for the ALE analysis, and all nodes are fixed for the comparative Lagrangian analysis. The specimen is loaded by applying horizontal displacements of 0.16 mm in 80 equal steps at the vertices of the specimen (imposed displacements are directed inward at the top edge and outward at the bottom edge); for the intermediate nodes at the vertical edges the enforced displacement is interpolated from these values. In this example, inhomogeneities arise due to non-linearity, where it is noted that the structural behaviour differs in tension and compression, thus elements will tend to concentrate in the compressive regions.

Three different finite element discretisations have been used, one of which is regular. The other two are distorted versions of the regular mesh. Fig. 12 shows the Lagrangian results for the three meshes, obtained by keeping $\tilde{\boldsymbol{\Phi}}$ fixed and thus $\boldsymbol{\varphi} \equiv \bar{\boldsymbol{\varphi}}$. On the left of Fig. 12, the material domains $\mathscr{B}_0$ with corresponding discrete material forces are shown, while on the right the corresponding spatial domains $\mathscr{B}_t$ is plotted. Different meshes lead to different discrete material force residuals. The total energy associated with these

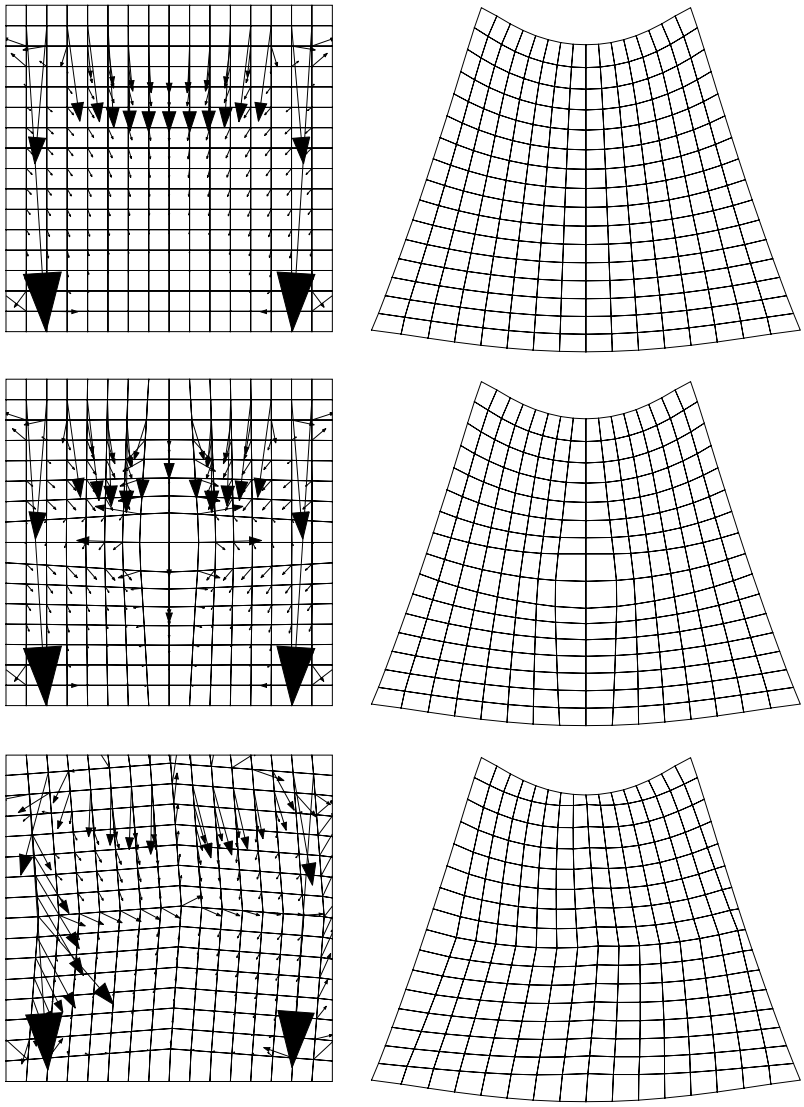

Fig. 12. Homogeneous block under bending—material domain $\mathscr{B}_0$ with material forces (left column) and spatial domain $\mathscr{B}_t$ (right column), Lagrangian analyses.

Lagrangian solutions is $\mathscr{I}^{\text{lagrange}} = 3657.3$ N mm, $\mathscr{I}^{\text{lagrange}} = 3657.7$ N mm and $\mathscr{I}^{\text{lagrange}} = 3655.8$ N mm, respectively. Clearly, the potential energies differ for the three meshes.

Fig. 13 illustrates the results of the ALE approach with $\tilde{\boldsymbol{\Phi}}$ free, thus nodes of $\mathscr{B}_0$ are allowed to move freely in space. The same results are obtained with all three meshes. Furthermore, all ALE analyses lead to a total potential energy $\mathscr{I}^{\text{ale}} = 3650.7$ N mm, which is (i) independent of the initial discretisation, and (ii) lower than the values obtained with either of the Lagrangian meshes. On the left of Fig. 13, the material domain $\mathscr{B}_0$ is shown. It is emphasised that here vanishing discrete material are found, since material node point positions are determined such that discrete material forces vanish identically. Fig. 14 demonstrates the development of the optimal material configuration $\mathscr{B}_0$ for the initially homogeneous mesh. Similar to

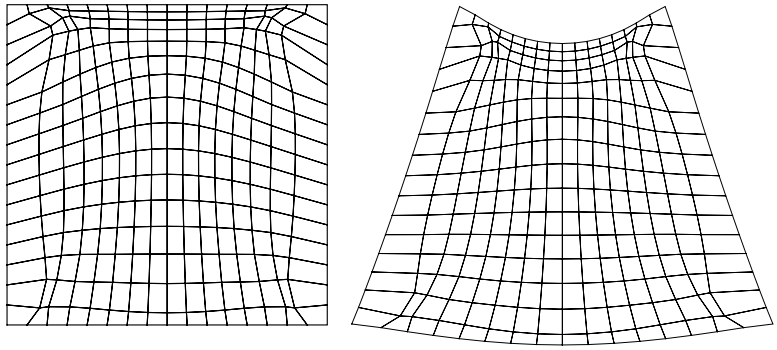

Fig. 13. Homogeneous block under bending—material domain $\mathscr{B}_0$ and spatial domain $\mathscr{B}_t$, ALE analysis.

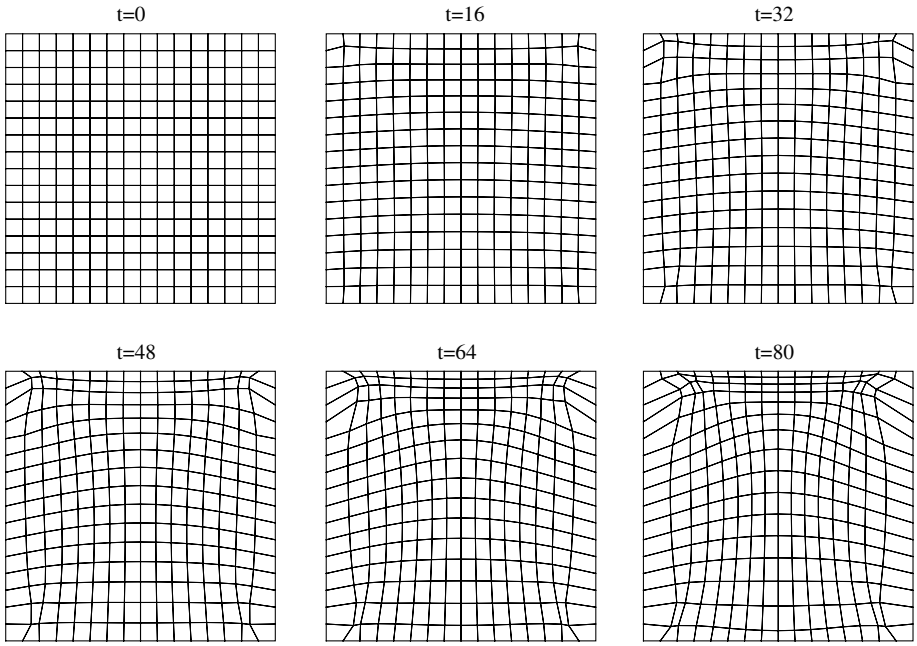

Fig. 14. Homogeneous block under bending—material domain $\mathscr{B}_0$, at different loading stages, ALE analysis.

the one-dimensional example of Section 5.1, it can be verified that the nodes have moved in the direction *opposite* to the discrete material forces found in Fig. 12 (left), Fig. 13 (right) shows the spatial domain $\mathscr{B}_t$ of the ALE solution.

Remark 9 (*Bending versus tension*). The bending problem, as compared to the tension problem of the previous section, is extremely elegant in the sense that inhomogeneity is introduced smoothly and discrete singularities which spoil the solution are avoided. Typically, special elements or higher-order elements have to be applied to study bending, so that locking phenomena are avoided. However, this is beyond the scope of the present contribution.

6. Conclusions

This contribution, consisting of two parts, is dedicated to the formulation of an arbitrary Lagrangian–Eulerian (ALE) method based on a dual equilibrium problem. In the first part, generic expressions for the spatial motion problem and the material motion problem have been derived in which the fundamental unknowns are the spatial as well as the material coordinates of the nodes. Since spatial forces and material forces are energy conjugated to variations in spatial coordinates and material coordinates, respectively, the dual equilibrium is intrinsically an ALE formulation. In terms of energy, the total potential energy of the system is minimised not only by optimising the spatial coordinates of the nodes (which is the standard procedure in Lagrangian mechanics) but also by optimising the material coordinates of the nodes.

In the present, second part of this contribution, applications within Neo–Hookean hyperelasticity are explored. To set the stage, several specifications of classical ALE formulations are discussed, including Total and Updated ALE descriptions and Monolithic (coupled) and Staggered (uncoupled) ALE algorithms. For the present application to hyperelasticity, a T-ALE scheme has the advantage that no convective terms appear in the governing equations, which greatly simplifies the implementation. Both M-ALE and S-ALE schemes are studied; comparisons for the one-dimensional case reveal that the use of a M-ALE scheme is more efficient from the point of view of CPU time, although larger matrices must be allocated.

The examples demonstrate that with the proposed ALE approach, potential energies are obtained that are the minimum that can be obtained with the considered finite element mesh topologies. In that sense, the ALE formulation based on the dual equilibrium is optimal, whereby it is emphasised that *no user parameters whatsoever* are needed in the mesh optimisation, in contrast to most other ALE methods from the literature. Thus, the ad hoc nature of most remeshing strategies is avoided in return for mesh optimisation based on energy considerations.

Though the formulation and implementation of hyperelasticity has been addressed in an as self-contained manner as possible, several aspects have not been addressed. Further study is needed for issues including the following:

- In this paper, only hyperelastic material of the Neo–Hookean type has been considered. The extension to time-dependent material behaviour includes thermomechanics, hyperelastoplasticity and inertia effects. Time updates invariably lead to convective effects, which must be accounted for.
- Incrementation of the residual in the material motion problem is not straightforward, as has been argued in Section 4.4. Although it constitutes a problem primarily in the very first load step, it requires a robust solution.
- Mesh optimisation based on vanishing discrete material forces aims at the minimisation of potential energy. Thus, in the terminology of Huerta and co-workers [37] the material force residual can be considered as a mathematically based *error estimator*, rather than an engineering-intuition based *error indicator*. Its relation with other error estimators of the flux-projection type [38] or of the residual type [39,40] could be studied.

References

[1] E. Kuhl, H. Askes, P. Steinmann, An ALE formulation based on spatial and material settings of continuum mechanics. Part 1: Generic hyperelastic formulation, Comput. Methods Appl. Mech. Engrg., previous article in this issue.
[2] G.A. Maugin, Material Inhomogeneities in Elasticity, Chapham & Hall, London, 1993.
[3] P. Steinmann, Application of material forces to hyperelastostatic fracture mechanics. I. Continuum mechanical setting, Int. J. Solids Struct. 37 (2000) 7371–7391.
[4] P. Steinmann, D. Ackermann, F.J. Barth, Application of material forces to hyperelastostatic fracture mechanics. II. Computational setting, Int. J. Solids Struct. 38 (2001) 5509–5526.

[5] R. Denzer, F.J. Barth, P. Steinmann, Studies in elastic fracture mechanics based on the material force method, Int. J. Numer. Methods Engrg. 58 (2003) 1817–1835.
[6] T. Liebe, R. Denzer, P. Steinmann, Application of the material force method to isotropic continuum damage, Comput. Mech. 30 (2003) 171–184.
[7] E. Kuhl, P. Steinmann, Material forces in open system mechanics, Comput. Methods Appl. Mech. Engrg. 193 (2004) 2357–2381.
[8] M. Braun, Configurational forces induced by finite-element discretization, Proc. Estonian Acad. Sci. Phys. Math. 46 (1997) 24–31.
[9] R. Mueller, G.A. Maugin, On material forces and finite element discretizations, Comput. Mech. 29 (2002) 52–60.
[10] P. Thoutireddy, M. Ortiz, A variational arbitrary Lagrangian–Eulerian (VALE) method of mesh adaption and optimization in static finite-element calculations, Int. J. Numer. Methods Engrg. 53 (6) (2002) 1337–1351.
[11] P. Thoutireddy, Variational arbitrary Lagrangian–Eulerian method, Ph.D. Thesis, California Institute of Technology, Passadena, California, 2003.
[12] H. Askes, E. Kuhl, P. Steinmann, Arbitrary Lagrangian–Eulerian (ALE) mesh optimisation by equilibration of discrete material forces, in: E. Oñate, D.R.J. Owen (Eds.), Computational Plasticity, CIMNE, Barcelona, 2003.
[13] J. Donéa, Arbitrary Lagrangian–Eulerian finite element methods, in: T. Belytschko, T.J.R. Hughes (Eds.), Computational Methods for Transient Analysis, Elsevier, 1983, pp. 474–516 (Chapter 10).
[14] T.J.R. Hughes, W.K. Liu, T.K. Zimmermann, Lagrangian–Eulerian finite element formulation for incompressible viscous flows, Comput. Methods Appl. Mech. Engrg. 29 (1981) 329–349.
[15] A. Huerta, F. Casadei, New ALE applications in non-linear fast-transient solid dynamics, Engrg. Comput. 11 (1994) 317–345.
[16] W.K. Liu, T. Belytschko, H. Chang, An arbitrary Lagrangian–Eulerian finite element method for path dependent materials, Comput. Methods Appl. Mech. Engrg. 58 (1986) 227–246.
[17] P.J.G. Schreurs, F.E. Veldpaus, W.A.M. Brekelmans, Simulation of forming processes, using the Arbitrary Eulerian–Lagrangian formulation, Comput. Methods Appl. Mech. Engrg. 58 (1986) 19–36.
[18] T. Yamada, F. Kikuchi, An arbitrary Lagrangian–Eulerian finite element method for incompressible hyperelasticity, Comput. Methods Appl. Mech. Engrg. 102 (1993) 149–177.
[19] A. Rodríguez-Ferran, A. Pérez-Foguet, A. Huerta, Arbitrary Lagrangian–Eulerian (ALE) formulation for hyperelastoplasticity, Int. J. Numer. Methods Engrg. 53 (2002) 1831–1851.
[20] F. Armero, E. Love, An arbitrary Lagrangian–Eulerian finite element method for finite strain plasticity, Int. J. Numer. Methods Engrg. 57 (2003) 471–508.
[21] F.P.T. Baaijens, An U-ALE formulation of 3-D unsteady viscoelastic flow, Int. J. Numer. Methods Engrg. 36 (1993) 1115–1143.
[22] A. Rodríguez-Ferran, F. Casadei, A. Huerta, ALE stress update for transient and quasistatic processes, Int. J. Numer. Methods Engrg. 43 (1998) 241–262.
[23] H. Askes, L. Bodé, L.J. Sluys, ALE analyses of localization in wave propagation problems, Mech. Coh.-Frict. Mater. 3 (1998) 105–125.
[24] G. Pijaudier-Cabot, L. Bodé, A. Huerta, Arbitrary Lagrangian–Eulerian finite element analysis of strain localization in transient problems, Int. J. Numer. Methods Engrg. 38 (1995) 4171–4191.
[25] H. Askes, A. Rodríguez-Ferran, A. Huerta, Adaptive analysis of yield line patterns in plates with the arbitrary Lagrangian–Eulerian method, Comput. Struct. 70 (1999) 257–271.
[26] S. Roels, J. Carmeliet, H. Hens, Mesh adaptive finite element formulations for moisture transfer in materials with a critical moisture content, Int. J. Numer. Methods Engrg. 46 (1999) 1001–1016.
[27] H. Askes, L.J. Sluys, Remeshing strategies for adaptive ALE analysis of strain localisation, Eur. J. Mech. A Solids 19 (2000) 447–467.
[28] H. Askes, A. Rodríguez-Ferran, A combined *rh*-adaptive scheme based on domain subdivision. Formulation and linear examples, Int. J. Numer. Methods Engrg. 51 (2001) 253–273.
[29] G. Rekers, Numerical simulation of unsteady viscoelastic flow of polymers, Ph.D. Thesis, University of Twente, 1995.
[30] J. Huétink, P.T. Vreede, J. van der Lugt, Progress in mixed Eulerian–Lagrangian finite element simulation of forming processes, Int. J. Numer. Methods Engrg. 30 (1990) 1441–1457.
[31] H. Wisselink, Analysis of guillotining and slitting—finite element simulations, Ph.D. Thesis, University of Twente, 2000.
[32] P.N. van der Helm, J. Huétink, R. Akkerman, Comparison of artificial dissipation and limited flux schemes in arbitrary Lagrangian–Eulerian finite element formulations, Int. J. Numer. Methods Engrg. 41 (1998) 1057–1076.
[33] H.C. Stoker, Developments of the arbitrary Lagrangian–Eulerian method in non-linear solid mechanics—applications to forming processes, Ph.D. Thesis, University of Twente, 1999.
[34] M.A. Gutiérrez, R. de Borst, J.C.J. Schellekens, L.J. Sluys, An algorithm for mesh rezoning with application to strain localization problems, Comput. Struct. 55 (1995) 237–247.
[35] D.S. McRae, *r*-Refinement grid adaptation algorithms and issues, Comput. Methods Appl. Mech. Engrg. 189 (2000) 1161–1182.
[36] J. Sarrate, A. Huerta, An improved algorithm to smooth graded quadrilateral meshes preserving the prescribed element size, Commun. Numer. Methods Engrg. 17 (2001) 89–99.

[37] A. Huerta, A. Rodríguez-Ferran, P. Díez, J. Sarrate, Adaptive finite element strategies based on error assessment, Int. J. Numer. Methods Engrg. 46 (1999) 1803–1818.
[38] O.C. Zienkiewicz, J.Z. Zhu, A simple error estimator and adaptive procedure for practical engineering analysis, Int. J. Numer. Methods Engrg. 24 (1987) 337–357.
[39] I. Babuška, C. Rheinboldt, A posteriori error estimates for the finite element method, Int. J. Numer. Methods Engrg. 12 (1978) 1597–1615.
[40] P. Díez, J.J. Egozcue, A. Huerta, A posteriori error estimation for standard finite element analysis, Comput. Methods Appl. Mech. Engrg. 163 (1998) 141–157.